Hindawi
Journal of Nanomaterials
Volume 2022, Article ID 2914210, 17 pages
https://doi.org/10.1155/2022/2914210

Research Article

Development of Chitosan-Assisted Fe_3O_4@SiO_2 Magnetic Nanostructures Functionalized with Nisin as a Topical Combating System against Vancomycin-Intermediate *Staphylococcus aureus* (VISA) Skin Wound Infection in Mice

Mona Nasaj,[1] Abbas Farmany,[2] Leili Shokoohizadeh,[1] Farid Aziz Jalilian,[3] Reza Mahjoub,[4] Ghodratollah Roshanaei,[5] Alireza Nourian,[6] Omid Heydari Shayesteh,[7] and Mohammad Reza Arabestani[1,8]

[1]*Department of Microbiology, Faculty of Medicine, Hamadan University of Medical Sciences, Hamadan, IR, Iran*
[2]*Dental Research Center, School of Dentistry, Hamadan University of Medical Sciences, Hamadan, Iran*
[3]*Department of Virology, Faculty of Medicine, Hamadan University of Medical Sciences, Shahid Fahmideh Street, Park Mardome, Hamadan, Iran*
[4]*Department of Pharmacology and Toxicology, School of Pharmacy, Medicinal Plants and Natural Products Research Center, Hamadan University of Medical Sciences, Hamadan, Iran*
[5]*Department of Biostatistics, School of Health, Hamadan University of Medical Sciences, Shahid Fahmideh Street, Park Mardome, Hamadan, IR, Iran*
[6]*Department of Pathobiology, School of Veterinary Science, Bu-Ali Sina University, Hamedan, Iran*
[7]*Department of Medicinal Chemistry, School of Pharmacy, Hamadan University of Medical Sciences, Hamadan, Iran*
[8]*Brucellosis Research Center, Hamadan University of Medical Sciences, Hamadan, IR, Iran*

Correspondence should be addressed to Abbas Farmany; a.farmany@alumni.ut.ac.ir
and Mohammad Reza Arabestani; mohammad.arabestani@gmail.com

Received 24 January 2022; Revised 30 March 2022; Accepted 8 April 2022; Published 28 April 2022

Academic Editor: Abdelwahab Omri

The clinical significance of vancomycin-intermediate *S. aureus* (VISA) infections is intensified by its tendency to develop resistance to antimicrobials and persistent infections. The decreasing effectiveness of the antimicrobials available is now seriously compromised; thus, there is an emergent need to invent new classes of antimicrobial agents that can rapidly and efficiently eradicate infections. Fe_3O_4@SiO_2@chitosan (CS) nanocomposites were successfully synthesized and then decorated with nisin to gain Fe_3O_4/SiO_2/CS/nisin-based magnetic nanostructures (Fe_3O_4@SiO_2@CS-NISIN). The nanomaterials were characterized comparatively via FTIR (Fourier transform infrared spectroscopy), XRD (X-ray diffraction), FE-SEM (field emission scanning electron microscopes), DLS (dynamic light scattering), and VSM (vibrating sample magnetometer) methods. The methyl thiazol tetrazolium (MTT) assay was performed to determine the inhibitory effects of antibacterial agents on the cell viability. The *in vitro* bactericidal effect of all compounds was characterized using the microdilution assay. Finally, the topical antibacterial efficacy of free nisin, Fe_3O_4@SiO_2@CS, and Fe_3O_4@SiO_2@CS-NISIN nanocomposites against murine superficial wound infection models was determined. The functionalized nanocomposites were more efficient in suppressing bacterial growth *in vitro* and *in vivo* compared to the same quantities of untargeted nanocomposites. MTT results showed acceptable biocompatibility of all nanoformulations, and no substantial difference in the cell viability was recorded between treated cells and untreated control. These results suggest that Fe_3O_4@SiO_2@CS-NISIN nanocomposites can be served as an alternative antimicrobial agent in innovative and emerging technologies to treat a variety of staphylococcal infections.

1. Introduction

Staphylococcus aureus (*S. aureus*) is strongly connected with a broad range of clinical problems, including skin and soft tissue infections to life-threatening diseases such as endocarditis and sepsis [1]. Infections with strains of MRSA are often resistant to methicillin and nearly all B-lactam antibiotics. In the 1980s, the treatment of MRSA infections began to shift towards the use of glycopeptide antibiotics, in particular vancomycin. Unfortunately, the pressure to use glycopeptide antibiotics resulted in the appearance of vancomycin-intermediate-resistant *S. aureus* (VISA), first reported in Japan in 1997. Since then, VISA has been increasingly isolated from hospitals around the world [2]. The *in vivo* development of strains with the intermediate level resistance to vancomycin, known as VISA, has resulted in treatment failure and prolonged hospitalization. Although VISA strains are known to be related to persistent bacteremia, they do not generally lead to critical clinical complications or lethal sepsis, indicating that reduced susceptibility to vancomycin may damage the pathogenicity of *S. aureus* [1]. In addition to the vancomycin-intermediated phenotype, VISA strains appear to share some common characteristics such as thickened cell walls, reduced autolytic activity, and impaired virulence traits [3]. Infections caused by VISA are more often associated with failure of vancomycin therapy and lead to prolonged hospitalization, a higher risk of persistent infection, and increased treatment costs [4, 5]. Thus, the successful treatment of these infections has become more difficult and remains a major challenge; therefore, it is an imperative need to develop modern strategies to counter MRSA/VISA infections. Nisin, a prototype of the lantibiotic group of antimicrobial peptides, has been approved by the US Food and Drug Administration (FDA) for application in the food industry. Nisin is found to exert bactericidal effects towards a great amount of Gram-positive bacterial organisms, including crucial food-borne pathogens and various clinically important antibiotic-resistant bacteria, such as *staphylococci*, bacilli, *mycobacteria*, and *clostridia*; in addition, nisin is also known to be activating autolytic responses in the *staphylococcal* cell wall [6]. Although nisin has much low or no effect against Gram-negative bacteria and fungi, its conjunction with other compounds such as chelating agents can extend its spectrum of action to include Gram-negative bacteria [7]. Nisin and other lantibiotics have attracted great attention because they are characterized by potent and broad-spectrum antimicrobial effects, a low tendency to develop bacterial resistance, and relatively slight toxicity to mammalian cells at antimicrobial concentrations [8–11]. Chitosan (CS) is recognized as the second most abundant hydrophilic amino biopolymer naturally appearing on earth, next to cellulose, and is made from marine crustacean shells [12, 13]. CS and its derivatives are being widely investigated for application in various fields of biomedical and drug delivery [14, 15], due to some useful features such as nontoxicity, biodegradability, biocompatibility, immunological neutrality, hydrophilicity, antimicrobial capacity, anti-inflammatory, antitumor, and wound healing effects [16]. Magnetic-based nanoparticles (MNPs) have recently attracted special consideration due to their distinct physicochemical properties, especially ready to modify and biocompatibility [17, 18]. MNPs have the capacity to carry high dosages of pharmaceutical agents, thus achieving effective topical content and avoiding toxic and other undesirable effects resulting from large doses of drugs in other parts of the body [19]. The most attractive advantage of MNPs in the drug delivery involves controlled release of the therapeutics at the target site via external magnetic fields, enhancing the accumulation of drugs at the site of cutaneous lesions and potentially improving therapeutic efficacy [20, 21]. The MNPs have a large surface area-to-volume ratio that yields numerous chemically active sites. High surface free energy can trigger the formation of nanoparticle agglomerates and decrease the available active sites [22]. Coating magnetic nanoparticles with organic or inorganic materials can reduce the surface magnetic force and avoid particle agglomeration [23]. An inorganic capping agent, namely, silica (SiO_2), with a low toxicity and the extraordinary physicochemical characteristics, is capable of improving stability and protecting the Fe_3O_4 MNPs from dissolution under acidic conditions, agglomeration, and chemical oxidation and also presents the suitable potential for modifying the surface [22, 24]. Some scientists found that naked Fe_3O_4-MNPs can trigger the generation of free hydroxyl radical species which interact with intracellular components such as endogenous DNA, resulting in impaired cellular function and proliferation [25, 26]. It has been documented that capping Fe_3O_4 MNPs by either inorganic materials (silica, gold) or synthetic/natural organic materials effectively prevents iron leaching in acidic intracellular degradation pathways and greatly improves the biocompatibility of metal particles for cellular applications, particularly at high magnetite loadings [27, 28]. In this work, we prepared Fe_3O_4 supermagnetic NP grafting with nisin to improve antibacterial property against VISA strain. Due to the ability to agglomerate, these nanoparticles are quickly removed from blood circulation through opsonization and phagocytosis by RES [29]. To prevent this issue, we should shield the surface of MNPs with biodegradable and biocompatible SiO_2 layer leading to increase stability. To enhance the surface characteristics of MNPs, we also employed the polycationic chitosan crosslinked with glutaraldehyde.

2. Materials and Methodology

2.1. Materials. Ferrous chloride ($FeCl_2{\cdot}4H_2O$), ferric chloride ($FeCl_3{\cdot}6H_2O$), ammonium hydroxide ($NH_3{\cdot}H_2O$, 25 wt%), hydrochloric acid (HCl, 35 wt%-37 wt%), sodium acetate ($C_2H_3NaO_2$), tetraethyl orthosilicate (TEOS), glutaraldehyde (25 wt%), ethanol (96%), and vancomycin hydrochloride were purchased from Sigma Aldrich (MO, USA). Polyethylene glycol (PEG-400), medium molecular weight chitosan (MMWC, deacetylation degree of 75–85%), nisin from *Lactococcus lactis* 2.5% (balance sodium chloride), blood agar, and Mueller-Hinton broth (MHB) were obtained from Merck (Darmstadt, Germany). Dulbecco's modified Eagle's medium (DMEM), fetal bovine serum (FBS), penicillin, and streptomycin were obtained from Gibco, USA. Male NMRI mice, 6–8 weeks old, were purchased from the Center

of Experimental and Comparative Study (Iran University, Tehran). We have also used Gram-positive bacteria vancomycin-intermediate *Staphylococcus aureus* (VISA), from Hamadan University of Medical Sciences, Hamadan, IRAN.

2.2. Preparation of Fe_3O_4 Magnetic Nanoparticles. Monodispersed Fe_3O_4 magnetic nanoparticles (MNPs) were synthesized based on the chemical coprecipitation method as already described with some modifications: typically, 4.6 g $FeCl_3{\cdot}6H_2O$, 2.3 g $FeCl_2{\cdot}4H_2O$, and 0.6 g PEG-400 were dissolved in 100 mL of 1.2 mmol/L aqueous HCl in an ultrasonic bath for 30 min (Elma, Germany), then incubated with vigorous mechanical stirring (500 rpm) at 80°C (Hot Plate, Pole Ideal Tajhiz, Iran), and exposed to a high-purity nitrogen atmosphere. After continued stirring for 30 min, 20 mL $NH_3{\cdot}H_2O$ (25%) containing 0.3 g PEG-400 solution was slowly poured dropwise into the reaction mixture over 20 min until reaching pH to the alkaline state, at which the solution color changed from brown to dark brown and then became black. Upon lowering the temperature of the mixture, the ultrafine MNPs were repeatedly washed at first with deionized water and then ethanol until their pH became neutral, followed by drying in a vacuum oven (Bionics Scientific Technologies (P) Ltd., India) at 70°C for 10 h [30].

2.3. Synthesis of the Fe_3O_4@SiO_2 Core/Shell Nanocomposites. The silica-coated Fe_3O_4 MNPs (Fe_3O_4@SiO_2) were prepared based on the sol-gel approach according to the previously reported works with modifications [31]. 2 g of synthesized Fe_3O_4 particles was initially dispersed into a 200 mL mixture comprising ethanol and deionized water (160 : 40) then subjected to ultrasonic irradiation for 15 min using a probe sonicator (Vibra-Cell™ Jencons Scientific Ltd., USA). 30 min after the addition of ammonia solution (4 mL, 25 wt%), 2 mL of TEOS was dropped into the reaction solution, and the resulting suspension was vigorously stirred for 6 h. Silica was formed on the surface of the MNPs through hydrolysis and condensation of TEOS. Subsequently, the Fe_3O_4/SiO_2 nanostructures were washed with ethanol (3 × 15 mL) and dried under vacuum at 60°C for 12 h.

2.4. Preparation of Chitosan-Coated Fe_3O_4@SiO_2 Nanocomposites. To prepare chitosan-modified Fe_3O_4@SiO_2 MNPs, the nanostructures (0.5 gr) were first dispersed in distilled water (30 mL) under ultrasonication vibration for about 30 min. Then, 70 mL of acetic acid (CH_3COOH) solution of CS (0.5 g CS in 100 mL 2% CH_3COOH) was added in a dropwise manner into the nanocomposites aqueous solution under constant mechanical stirring at 50°C. The stirring of the reaction mixture was continued for about 3 h, followed by crosslinking of the nanocomposites with 2.5% glutaraldehyde at 40°C for 2 h to increase their mechanical and chemical stability. Finally, the chitosan/magnetite nanoparticles were recovered from the solution with a strong neodymium magnet; after that, the precipitated product was rinsed with ethanol several times, and the drying process was accomplished under vacuum at 60°C for 2 h [32].

2.5. Preparation of Calibration Curve of Nisin. Nisin solutions with different concentrations of 62.5, 125, 250, 500, 1000, and 2000 μg/mL were prepared separately by dissolving 562.5 μg, 1.125 mg, 2.25 mg, 4.5 mg, 9, and 18 mg nisin in 9 mL of phosphate buffer saline (PBS, pH 7.4), 9 mL of Tris buffer (pH, 9.5), and 9 mL of sodium acetate buffer (pH, 9.5), followed by adding 1 mL of Coomassie Brilliant Blue solution as the chromogenic agent to each mixture solution; three mixtures containing 9 mL each of buffer solutions and 1 mL Brilliant Blue dye were considered as control. Subsequently, a UV-Vis spectrophotometer (SPECORD 205, Analytik Jena, China) was employed to determine the absorbance of each mixture solution at 595 nm [33].

2.6. Modification of Fe_3O_4@SiO_2@CS Nanocomposites with Nisin. Covalent binding of nisin onto Fe_3O_4@SiO_2@CS nanocomposites was achieved by dropping 50 μL of glutaraldehyde (25% *v*/*v*) into the particle suspensions (2000 μg of Fe_3O_4@SiO_2@CS in 150 μL of sodium acetate buffer, 50 mM, pH 5.5), and the resulting suspension was allowed to proceed by shaking at 80 rpm for 1 h (Shaking Incubator (SI-100 R), Hanyang Scientific Equipment Co., Ltd., Korea). Thereafter, the samples were collected using twice washings with sodium acetate buffer (50 mM, pH 5.5), followed by rapid addition of a predetermined amount of nisin (2000 μg) to the activated Fe_3O_4@SiO_2@CS suspensions. Shaking was continuous overnight at 25°C. At the end of the experiment, excessive nisin removal and triplicate washings were carried out using an acetate buffer solution and centrifugation (Centrifuge 5425, Eppendorf North America Co, US), at 13000 × g for 20 min [34].

2.7. Determination of the Binding Efficiency of the Fe_3O_4@SiO_2@CS Nanocomposites. The nisin-loaded Fe_3O_4@SiO_2@CS composites were collected by ultrafiltration technique (Amicon, Ultracel-100 K, 100 kDa cutoff) after centrifuging at 2000 × g and 4°C for 15 min to separate the uncoated peptides from the nanoparticles (Centrifuge 5920 R, Eppendorf North America Co, US). The residual nisin content in the outer tube was measured using Bradford protein assay with a UV-Vis microspectrophotometer (Synergy HTX, BioTek com, US) at a wavelength of 595 nm. Three repeats of all experiments were considered, and the average absorbance values were calculated; the final amount of loaded nisin was calculated indirectly with [35, 36]

$$\text{Loading rate\%} = \frac{\text{nisin total} - \text{nisin supernatant}}{\text{nisin total}} \times 100. \quad (1)$$

2.8. In Vitro Release Profile of Nisin from the Nanocomposites. The nisin-loaded nanocomposites were separated from the aqueous suspension using the ultracentrifugation technique at 2000 × g for 20 min at 4°C; in the experiment, 20 mL of Fe_3O_4@SiO_2@CS-NISIN composite solution in Tris buffer (pH 9.5, 4 mg/mL) and phosphate-buffered saline (PBS, pH: 7.4, 4 mg/mL) was separately poured into a conical flask containing 50 mL dissolution medium and incubated at 25°C under continuous stirring (100 rpm, 24 h). At appropriate intervals of 0, 30, 60, 120, 240, 300, 360, 420, and 520 min, 5 mL of the solution was used for withdrawal accompanied by simultaneous replacement of an equal volume of fresh

medium, loaded into an ultrafiltration tube (M.W. cutoff of 30 kDa) and centrifuged at $2000 \times g$ for 20 min to remove possible insoluble constituents. After centrifugal separation, the nisin concentration in the supernatant was analyzed by the Bradford method, all release tests were performed in triplicate, and the mean value was reported [37, 38].

2.9. Characterization Methods. Chemical modification of Fe_3O_4 MNPs (Fe_3O_4@SiO_2, Fe_3O_4@SiO_2@CS, and Fe_3O_4@SiO_2-CS-NISIN) was characterized using the Fourier transform infrared (FT-IR) spectra of the nanocomposites on an FTIR spectrometer (Bruker Co., Germany) with a resolution of 4 cm^{-1} in the range 4000–400 cm^{-1} using KBr pellets. The magnetic properties of Fe_3O_4, Fe_3O_4@SiO_2, Fe_3O_4@SiO_2 @CS, and Fe_3O_4@SiO_2@CS-NISIN nanocomposites were evaluated at room temperature (300 K) using a vibrating sample magnetometer (VSM, Quantum, USA). The X-ray diffraction (XRD) patterns of Fe_3O_4 and Fe_3O_4@SiO_2@CS-NISIN composite nanoparticles were collected using an X-ray diffractometer (D8 ADVANCE, Bruker, Germany). A field emission scanning electronic microscope (FE-SEM, TSCAN, Czech Republic) was employed to evaluate the surface morphological characteristics and size of Fe_3O_4 and Fe_3O_4@SiO_2 MNPs. Before measurements, the samples were covered with a conductive gold layer to avoid charging issues during examination. Hydrodynamic size and zeta potential measurements were detected via dynamic light scattering (DLS) technique using Zetasizer Nano ZS 3600 (Malvern, Worcestershire, United Kingdom).

2.10. In Vitro Antibacterial Behavior of Therapeutic Agents

2.10.1. Determination of Minimum Inhibitory Concentration (MIC) and Minimum Bactericidal Concentration (MBC). To measure the MIC and MBC values of Fe_3O_4@SiO_2, Fe_3O_4@SiO_2@CS, nisin, and Fe_3O_4@SiO_2@CS-NISIN against the VISA strain, a standard broth microdilution susceptibility testing procedure was conducted using Mueller-Hinton broth (MHB) as recommended by the Clinical and Laboratory Standards Institute (CLSI) [39]. Briefly, the composites and nisin were diluted in 2-fold increments; for free nisin and Fe_3O_4@SiO_2@CS-NISIN nanocomposites, different concentrations were prepared in the range of 768–12 μg/mL, and for Fe_3O_4@SiO_2 and Fe_3O_4@SiO_2@CS nanocomposites, concentrations ranged from 4000 to 125 μg/mL. A previously prepared culture of VISA (OD_{625} of 0.5) was diluted to a final concentration of 10^6 CFU/mL in MHB culture. The bacterial inocula and prepared antimicrobial compound dilutions were added in a 1 : 1 ratio to individual wells of a 96-well microplate and then incubated for 24 h at 37°C (Incubator KB, BINDER Inc., US). The lowest concentration of the antimicrobial substance at which by visual reading the microorganism growth was completely inhibited was determined as the MIC value. To estimate the MBC of the antimicrobials, a viable cell count was carried out: briefly, the bacterial suspensions (10 mL) of each well, considered as the MIC value, were spread on the MH agar plates, followed by bacterial colony count after incubation at 37°C for 24 h. The lowest antimicrobial concentration, where more than 99.9% of the total bacterial population was killed, was termed the MBC endpoint.

2.11. The Cell Viability Assessment. The *in vitro* cytotoxicity effects of materials were identified by MTT assay in mouse L-929 fibroblast cells. Briefly, the cells were plated overnight into 96-well microtiter plates (Sigma, Germany) at a cell density of 1×10^5 cells per well with a volume of 200 μL complete DMEM, incubated at 37°C under an atmosphere of 5% CO_2. Cells were then exposed to various treatments with the nanocarriers: 125, 250, 500, 1000, 1500, 2000, and 4000 μg/mL Fe_3O_4, Fe_3O_4@SiO_2, Fe_3O_4@SiO_2@CS; 12, 24, 48, 96, 192, 384, and 768 μg/mL free nisin and Fe_3O_4@SiO_2@CS-NISIN composites. Following 24 hours of incubation at 37°C, each well was carefully resuspended in 10 μL of a 5 mg/mL MTT solution, and the plates were incubated for an additional four hours at 37°C, after which the MTT solution was removed from each well. The viable cells were exposed to 100 μL of dimethyl sulfoxide (DMSO) (Millipore Sigma) to solubilize the purple formazan crystals formed in the cells. After gently shaking the plate for 15 min with an orbital shaker (ES 20, Labortechnik, Germany), the absorbance of the wells was recorded with a microplate reader (680 XR, Bio-Rad, USA) at $\lambda_{max} = 570$ nm to calculate cell viability.

2.12. Animal Studies. The *in vivo* antibacterial efficacy of nisin, Fe_3O_4@SiO_2@CS, and Fe_3O_4@SiO_2@CS-NISIN nanocomposites was evaluated in the healing of full-thickness wounds of mice according to the international guidelines' principles of laboratory animal use and care [40]. Male NMRI mice, 6-8 weeks old, were divided into three groups (8 animals per group): nisin, Fe_3O_4@SiO_2@CS, and Fe_3O_4@SiO_2@CS-NISIN nanocomposites. Animals were kept under sanitary circumstances in a laboratory with a temperature of 22–25°C, a humidity of 40–70%, a light/dark cycle of 12 h, and free access to standard rodent feed and water ad libitum. After 2 weeks of acclimation, the animals were anesthetized with ketamine (40 mg/kg, Woerden, Netherlands) and xylazine (20 mg/kg, Woerden, Netherlands) through intraperitoneal injection. Afterward, a shaved area of the skin on the animal back was disinfected with 70% ethanol, and full-thickness circular excisions (7 mm diameter) were created on the dorsal midline of the animal using a sterile 4 mm biopsy punch, after which 100 μL of a bacterial suspension at a concentration of 3×10^8 CFU/mL was immediately introduced into each wound site. Treatment was performed according to the MIC dose for Fe_3O_4@SiO_2@CS composites and at considerably greater dosages (4-fold higher than the MIC concentrations) of nisin (96 μg/mL) and Fe_3O_4@SiO_2@CS-NISIN nanocomposites (500 μg/mL) to evaluate the antibacterial capacity to achieve a therapeutic effect *in vivo*. Nisin and Fe_3O_4@SiO_2@CS composites were administered every 12 hours. However, Fe_3O_4@SiO_2@CS-NISIN nanocomposites were used as a single daily dose. Subsequently, on days 4, 9, and 14, the mice were anesthetized and sacrificed, tissues from the wound area were harvested, and after homogenization, the bacterial cell count was determined.

2.13. Statistical Analysis. The variance (ANOVA) procedure and Tukey analysis are used for comparing the differences between relevant groups mean and to describe the possible relationship between variables. All tests were conducted in triplicate, and the differences of the mean findings had to be accepted at the significant level p lower than 0.05.

3. Results

3.1. FE-SEM Analysis. The FE-SEM analysis was used to evaluate the particle size and microstructure of the samples, and the micrographs of each sample at different magnifications are shown in Figure 1. As shown in Figure 1, quasi-spherical nanoparticles with different size ranges can be observed in all the samples. To determine the particle size of the samples, 100 particles were measured from each sample using ImageJ software, and histograms of the particle size distribution of these measurements are shown in Figure 2. According to the histograms shown in Figure 2, 25% of the Fe_3O_4 particles measured were in the range of 25-30 nm in diameter. The histogram of Fe_3O_4@SiO_2@CS-NISIN nanocomposites showed that the greatest number of particles was concentrated in the size range of 40 to 45 nm, with a frequency of 20-24%. Statistical data obtained from these measurements are reported in Table 1. It revealed that Fe_3O_4@SiO_2@CS-NISIN nanocomposites had a larger particle size, with an average particle size of 47.25 than Fe_3O_4 which had an average size of 28.55 nm. This may be due to the adsorption of organic agents on the surface of MNPs. It is also clear that the standard deviation in the particle size distribution for the samples of Fe_3O_4@SiO_2@CS-NISIN and Fe_3O_4 was equal to 11.14 and 6.4 nm, respectively. The higher standard deviation values in the nisin-modified nanocomposites indicate a wider size distribution for these samples. In other words, the particle size values of the modified nanocomposites were further deviated from the average value compared to the Fe_3O_4 particles.

3.2. FTIR Analysis. Figure 3 represents the FT-IR spectra of Fe_3O_4, Fe_3O_4@SiO_2, Fe_3O_4@SiO_2@CS, and Fe_3O_4@SiO_2@CS-NISIN nanocomposites. As shown in the spectra of Fe_3O_4, the typical absorption peaks concentrated at 468-571 cm^{-1} correspond to the stretching of the Fe–O or O-Fe-O associated with the magnetite phase of nanoparticles [41, 42]. The IR spectra of Fe_3O_4@SiO_2 revealed an absorption band around 995 cm^{-1} associated with an asymmetric stretching vibration Si–O or Si–OH, suggesting the successful formation of a silica layer on the surface of Fe_3O_4 [43]. The spectra of the synthesized Fe_3O_4@SiO_2@CS nanocomposites displayed a band concentrated at 1104 cm^{-1} that attributed to stretching vibrations of C-O and C-N bonds and a band at around 1411 cm^{-1}, which can be regarded as stretching modes of C–H, confirming the presence of the –CH and $–CH_2$ groups in the chitosan. The characteristic band at 1610 cm^{-1} is due to the O-H bending modes of water molecules and also to stretching vibrations of the N-H bond, confirming the existence of the $–NH_2$ functional group in the chitosan. The absorption bands in the regions 2850 and 2923 cm^{-1} are attributed to the stretching vibrations of the C-H bond of the chitosan structure. As can be indicated in the corresponding spectra of Fe_3O_4@SiO_2@CS-NISIN, the absorption bands detected between 1072 and 1238 cm^{-1} are described as C-O and C-N stretching modes of the chitosan structure. The absorption bands identified at 1454 cm^{-1}, arising from the C-H stretching vibrations, indicate the $-CH_3$ and -CH groups of chitosan and the aromatic C-C bond (Ar C-C) of the nisin structure. The band located at 1623 cm^{-1} refers to O-H bending vibrations of H_2O molecules and also stretching vibrations deriving from the N-H bond of the $-NH_2$ group. The emerging band at 1731 cm^{-1} is caused due to the vibrations of the C=O bond in the nisin structure, which confirm the appearance of nisin in the sample structure. The peak in the region 2923 cm^{-1} indicates stretching vibrations of the C-H group in chitosan and nisin. The peak stretching around 3428 cm^{-1} corresponds to O-H vibrational properties of H_2O molecules absorbed into Fe_3O_4 and the O-H groups in chitosan and nisin.

3.3. XRD Analysis. Figure 4 displays the X-ray diffraction (XRD) patterns of the Fe_3O_4 and Fe_3O_4@SiO_2@CS-NISIN nanostructures. The six characteristic peaks of Fe_3O_4 at 2θ = 30.3°, 35.7°, 43.4°, 53.9°, 57.3°, 62.8°, and 74.6° are related to their respective indices (220), (311), (400), (442), (511), (440), and (533), respectively, indicating the typical characteristics of Fe_3O_4 with a cubic spinel structure (JCPDS No. 00-075-0449). Meanwhile, following surface functionalization with the SiO_2 layer, chitosan, and nisin, the intensity of the Fe_3O_4 corresponding peaks noticeably decreased, indicating that the content of Fe_3O_4 in these nanocomposites was decreasing. The crystalline size of the Fe_3O_4 and Fe_3O_4@SiO_2@CS-NISIN particles was calculated using the Scherrer equation [44].

$$D = \frac{K\lambda}{\text{FWHM}} \times \cos(\theta), \tag{2}$$

where D is the crystalline size, K is the shape factor, λ is the X-ray wavelength used (1.54°A), FWHM is the bandwidth at half-height, and θ is the peak position. Given the values of $\cos(\theta)$ and FWHM, as well as the constant values of λ (1.54°A) and K (0.9), the crystalline size is obtained according to the Scherrer equation. The crystalline size values are calculated to be 54.8 and 22.34 nm for Fe_3O_4 and Fe_3O_4@SiO_2@CS@NISIN composites, respectively. The reduced crystalline size of nanomaterials containing organic compounds may be due to the capping of these compounds to the crystalline planes and preventing the growth of the crystal structure during the nucleation and the growth processes of the MNPs.

3.4. DLS Analysis. The surface electric charge (zeta potential) of particles dispersed in a colloidal media is an important indicator of the stability of the colloid [45]. It is generally argued that a lower absolute value of the zeta potential suggests a lower stability of colloidal systems, and absolute values of the potential above 30 mV indicate a stable suspension [46]. The zeta potential values for Fe_3O_4, Fe_3O_4@SiO_2, and Fe_3O_4@SiO_2@CS nanomaterials were around -14.25 mV,

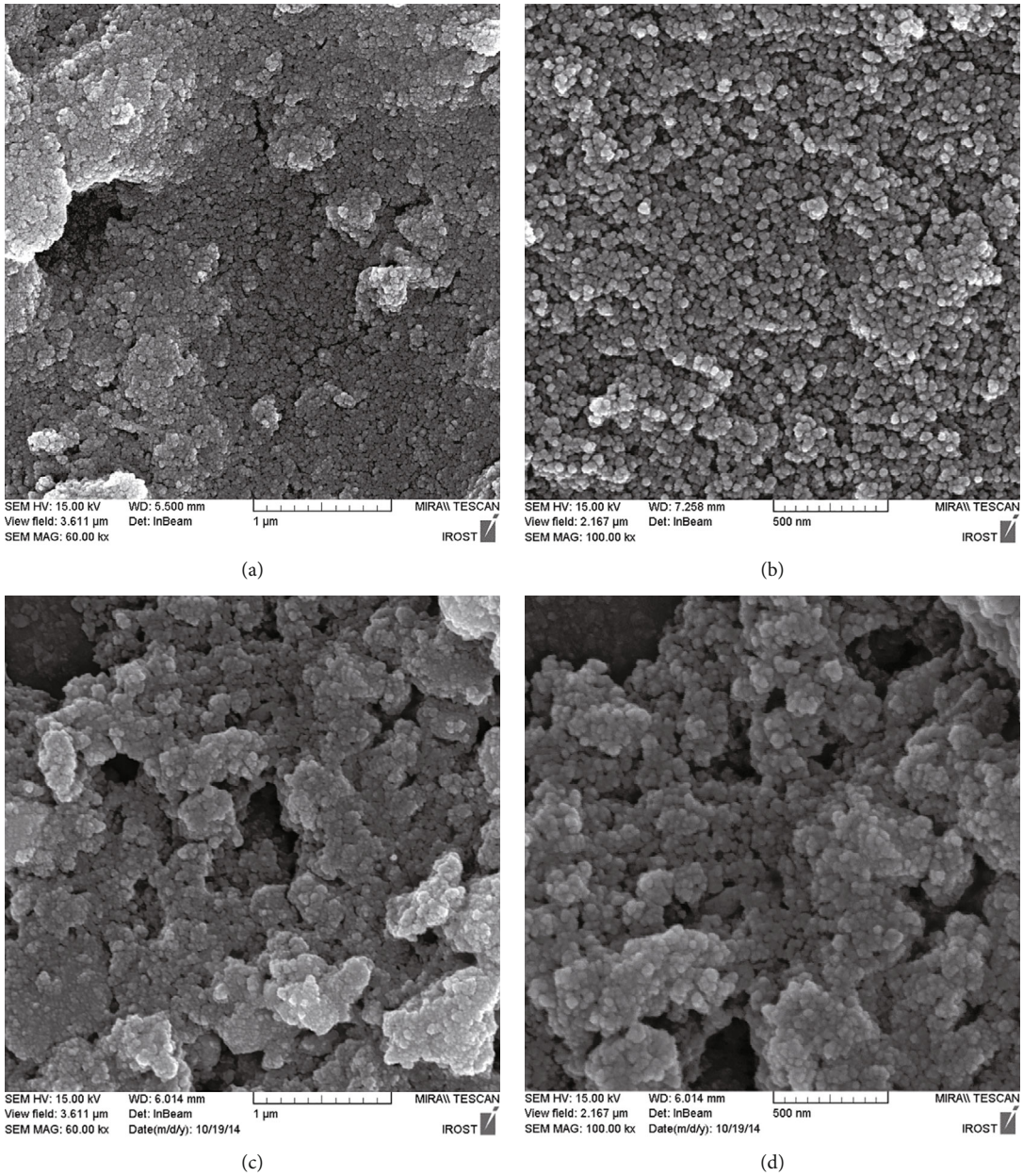

Figure 1: SEM images of (a, b) Fe_3O_4 and (c, d) Fe_3O_4@SiO_2@CS-NISIN at 60000 and 100,000 magnifications.

-7.19 mV, and 31.74 mV, respectively. The zeta potential values obtained suggest that, among the underexamined samples, only Fe_3O_4@SiO_2@CS had an absolute zeta potential value of more than 30 mV. Therefore, it can be concluded that Fe_3O_4@SiO_2@CS is a stable suspension. The hydrodynamic diameter (D_h) of all nanomaterials was recorded using the dynamic light scattering (DLS) method. The hydrodynamic diameters of Fe_3O_4 and Fe_3O_4@SiO_2 nanostructures are calculated to be around 51.4 and 93.7 nm, respectively. The hydrodynamic diameters of the nanostructures were obtained to be larger than those calculated from SEM measurements due to the presence of hydrated layers on the surfaces in aqueous media. After surface modification with CS and nisin, due to the reduced dispersion of the nanostructures, the diameters of the Fe_3O_4@SiO_2@CS and Fe_3O_4@SiO_2@CS-NISIN nanocomposites increased up to 129.5 and 155.8 nm, respectively, confirming the successful modification of the silica shell using CS and nisin.

3.5. VSM Analysis. As represented in Figure 5, magnetic hysteresis curves were calculated at 25°C to assess the magnetic behavior of the synthesized nanoparticles. The amount of saturated magnetization (Ms) of Fe_3O_4, Fe_3O_4@SiO_2, Fe_3O_4@SiO_2@CS, and Fe_3O_4@SiO_2@CS-NISIN reached 66.5 emu/g, 47.3 emu/g, 36.4 emu/g, and 26.7 emu/g, respectively. A significant reduction in the saturation magnetization degree from Fe_3O_4 to Fe_3O_4@SiO_2@CS-NISIN has been absolutely associated with the existence of nonmagnetic components, which are gradually added onto the surface of Fe_3O_4 magnetic nanoparticles such as SiO_2, CS, and

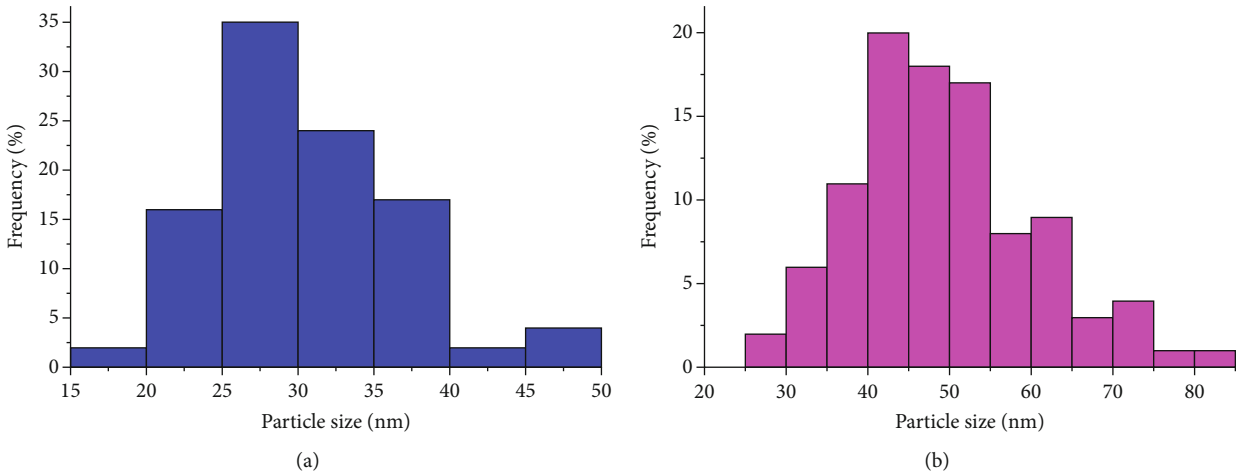

Figure 2: Particle size distribution histograms of (a) Fe_3O_4 and (b) Fe_3O_4@SiO_2@CS-NISIN nanocomposites.

Table 1: Statistical results of histograms of the understudied samples.

Sample	Number of the measured particles	Average particle size (nm)	Standard deviation (nm)	The smallest measured particle (nm)	The measured particle with medium size (nm)	The largest measured particle (nm)
Fe_3O_4	100	28.55	6.40	17.43	29.07	47.90
Fe_3O_4@SiO_2@CS-NISIN	100	47.25	11.14	24.43	48.85	82.18

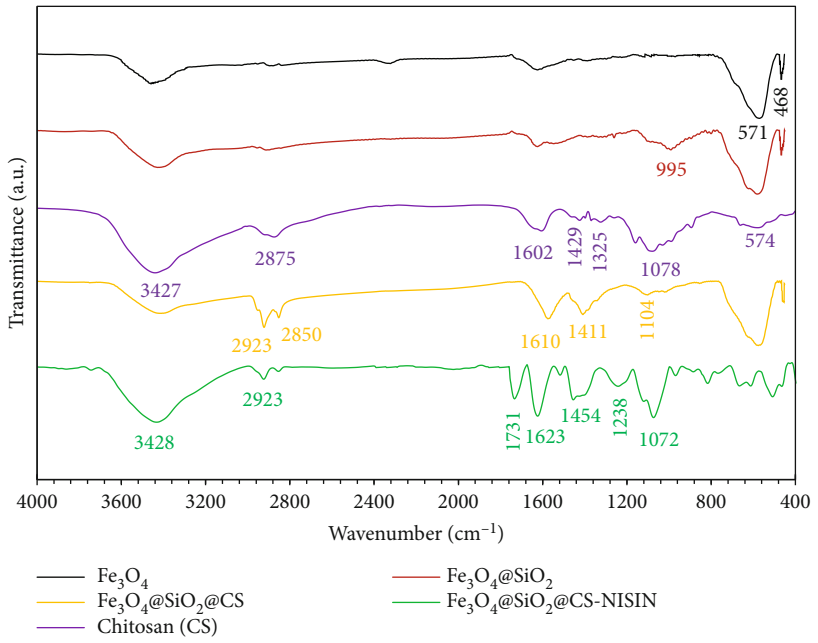

Figure 3: The FTIR spectra of synthesis materials Fe_3O_4, Fe_3O_4@SiO_2, chitosan (CS), Fe_3O_4@SiO_2@CS, and Fe_3O_4@SiO_2@CS-NISIN nanocomposites.

nisin, which was also in accordance with the DLS and FT-IR analyses. We found that the residual magnetic force in Fe_3O4@SiO_2@CS-NISIN nanocomposites was large enough to separate a valuable portion of nanovesicles under an external magnetic field, although the degree of saturation magnetization decreased. According to the above observation, Fe_3O_4@SiO_2@CS-NISIN nanocomposites exhibited appropriate dispersibility and magnetic response in water, making them suitable for magnetically targeted applications. Following our results, the studied nanocarriers are isotropic

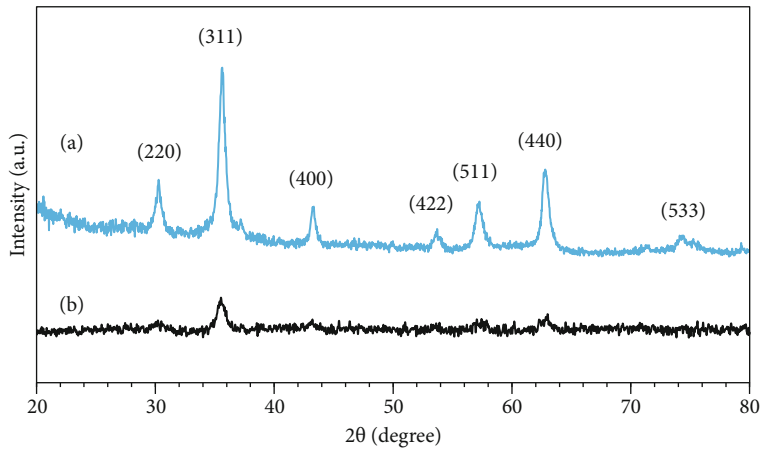

Figure 4: The XRD patterns of (a) Fe_3O_4 and (b) Fe_3O_4@SiO_2@CS-NISIN nanocomposites.

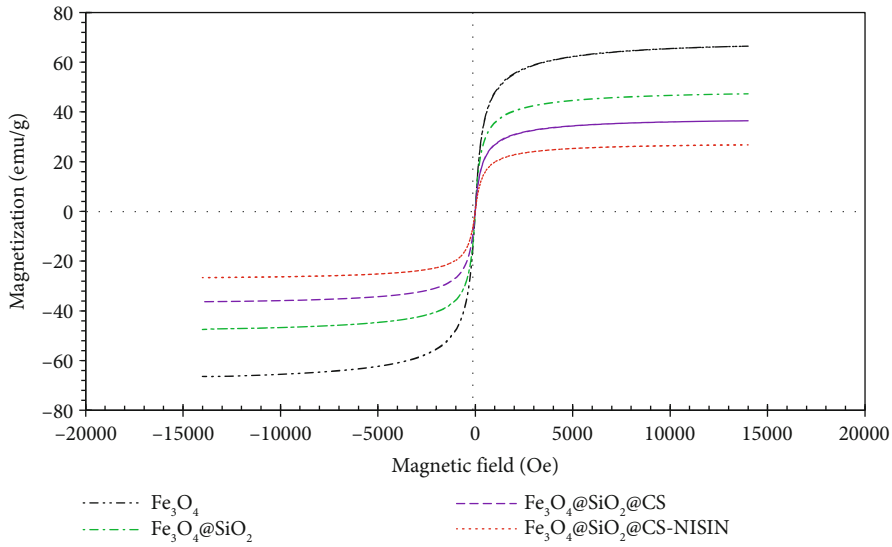

Figure 5: VSM magnetization curves of the obtained Fe_3O_4, Fe_3O_4@SiO_2, Fe_3O_4@SiO_2@CS, and Fe_3O_4@SiO_2@CS-NISIN, respectively.

and display superparamagnetic behaviors, and the coercivity and remanent magnetization of all nanomaterials are equal to zero.

3.6. Preparation of Calibration Curves of Nisin. The linear regression equations for the calibration curves were obtained as follows: $Y = 0.0001x + 0.0176$ ($R^2 = 0.998$), which was prepared based on sodium acetate buffer to estimate loading nisin. $Y = 0.0001x + 0.0267$ ($R^2 = 0.998$) and $Y = 0.0001x + 0.0203$ ($R^2 = 0.996$) were obtained using PBS and Tris buffers, respectively, to determine the *in vitro* release profile of nisin, where X is nisin concentration (μg/mL) and Y is absorbance (Figure 6).

3.7. Release Profile and Covalent Binding Rate of Nisin onto Nanoparticles. The profiles of nisin release under *in vitro* conditions after 120 h incubation at the phosphate-buffered saline (PBS, pH 7.4) and Tris buffer (pH 9.5) are presented in Figure 7. The results confirmed the greater release rate of nisin over the first 20 h, after which it slowly reduced over time. Of interest to note is that during the initial and transitional release, more than 51% and 96% of the protein molecules were released into PBS and Tris buffer, respectively. After this phase, the release slowed down until it reached a steady state as expected (Figure 7). The results revealed that the release rate of nisin was greater in Tris buffer than that of PBS buffer. The higher release rate of nisin in Tris buffer (pH 9.5) can be ascribed to the high negative charge density of nisin when the pH is greater than the isoelectric point (PI, 8.5). Thus, nisin molecules with a net negative surface charge under such conditions are readily separated from surfaces bearing a negative charge in the Tris buffer. On the other hand, a slower release rate of nisin from Fe_3O_4@SiO_2@CS composites was observed in PBS buffer (pH 7.5), which is due to the fact that nisin has a higher density of positive charge at this pH than at pH 9.5. The high level of positive charge leads to the slower release of nisin from the negatively charged nanocomposites in PBS buffer. In conclusion, the

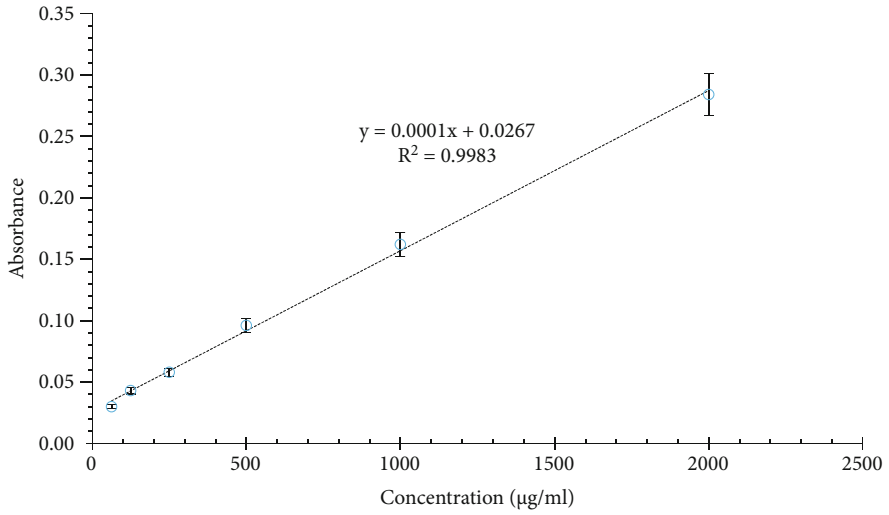

Figure 6: The standard calibration curve for nisin dissolved in PBS buffer (pH, 7.4).

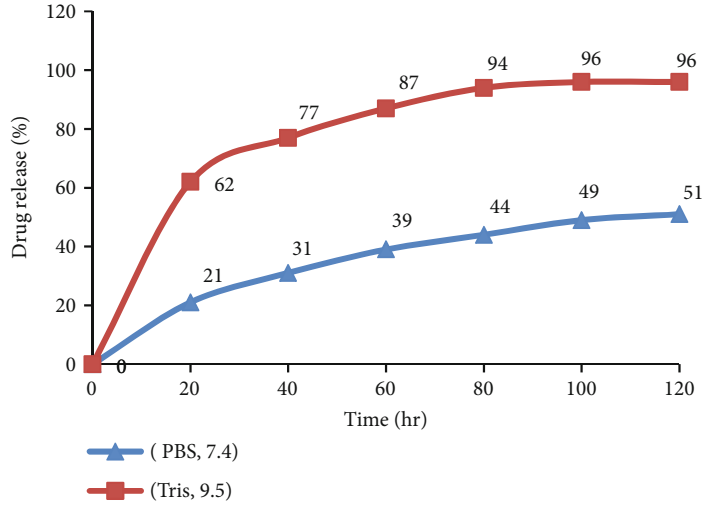

Figure 7: The *in vitro* nisin release profile of Fe_3O_4@SiO_2@CS nanocomposites in PBS (pH 7.4) and Tris (pH 9.5) buffers at 37°C.

findings suggest that the nanocomposites are capable of controlling the release of conjugated peptides. The covalent binding rate was measured to be 73.2%-85.2%, which was determined using the equation $y = 0.0001x + 0.0176$ obtained through the preparation of a nisin calibration curve using sodium acetate buffer (50 mM, pH 5.5).

3.8. Antibacterial Assessment of Manufactured Nanoparticles. In our analyses, we found that the antibacterial efficiency of the CS-coated Fe_3O_4@SiO_2 MNPs is partially greater ($p \leq 0.05$) than that of the unmodified Fe_3O_4@SiO_2 particles (Table 2). The treatment with Fe_3O_4@SiO_2@CS showed that the incorporation of chitosan onto the particles could further increase the sensitivity of the VISA strain against such nanostructures, as the chitosan-coated MNPs were capable of reducing both the MIC and MBC concentrations up to 2-fold when compared to free MNPs. The MIC and MBC ranges of Fe_3O_4@SiO_2 MNPs were estimated to be around 500 and 1000 μg/mL, respectively, whereas Fe_3O_4@SiO_2@CS composites exerted the bacteriostatic and bactericidal effects at the concentrations of 250 and 500 μg/mL, respectively. Nisin appeared to be extremely efficient against VISA strain as compared to two other compounds, with considerably lower MIC and MBC values (>24 μg/mL). It should be noted that the antibacterial capacity of the nisin-functionalized nanocomposites was greatly impaired when compared to free nisin, which can be explained due to the inactivation of some nisin molecules when covalently conjugated onto the Fe_3O_4@SiO_2@CS nanocomposites, significantly limiting the antibacterial property of the peptide. Free nisin could reduce the MIC and MBC values about 8-fold over the nisin-decorated nanocomposites (MIC/MBC of Fe_3O_4@SiO_2@CS-NISIN = 125 μg/mL, whereas free nisin had MIC/MBC > 24 μg/mL).

3.9. Cytotoxicity Activity of the Nanoparticles. We employed a standard MTT assay using various treatment concentrations of Fe_3O_4, Fe_3O_4@SiO_2, and Fe_3O_4@SiO_2@CS (125-

Table 2: MIC and MBC of different concentrations of $Fe_3O_4@SiO_2$, $Fe_3O_4@SiO_2@CS$, nisin, $Fe_3O_4@SiO_2@CS$-NISIN, and vancomycin.

Microorganism	Antibacterial agents									
	$Fe_3O_4@SiO_2$ (μg/mL)		$Fe_3O_4@SiO_2@CS$ (μg/mL)		Nisin (μg/mL)		$Fe_3O_4@SiO_2@CS$-NISIN (μg/mL)		Vancomycin (μg/mL)	
	MIC	MBC	MIC	MBC	MIC	MBC	MIC	MBC	MIC	MBC
VISA	500	1000	250	500	>24	>24	125	125	8	8

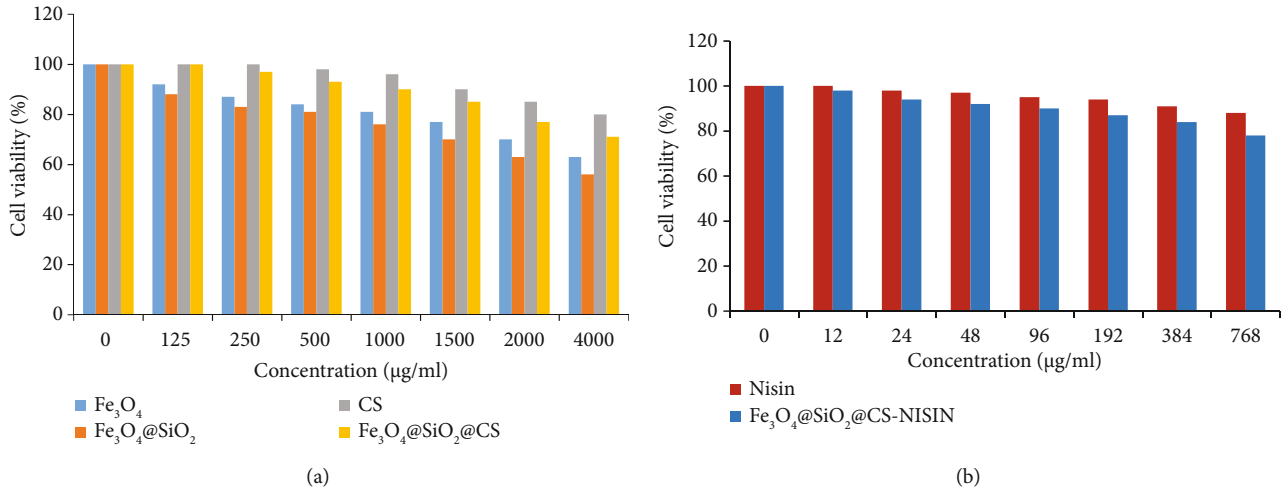

Figure 8: Representation of the cell viability rate of the L-929 cells after 24 hours following exposure with different treatments of (a) Fe_3O_4, Fe_3O_4@SiO_2, chitosan (CS), and Fe_3O_4@SiO_2@CS nanocarriers and (b) nisin and Fe_3O_4@SiO_2@CS-NISIN.

4000 μg/mL); nisin and Fe_3O_4@SiO_2@CS-NISIN nanocomposites (12-768 μg/mL) to evaluate the *in vitro* cytotoxic effects of the as-synthesized materials. Figure 8 shows the viability profile of the L-929 mouse fibroblast cells treated with the as-prepared compounds after a 24 h incubation. It can be seen that Fe_3O_4 MNPs presented no noticeable cytotoxicity effects even until a high exposure level, such as 4000 μg/mL, at which the cell viability achieved 63%, indicating the excellent cytocompatibility of Fe_3O_4 MNPs. The dose-dependent toxicity of Fe-O-based nanoparticles may be related to the further release of iron ions into the intracellular space during particle degradation. Furthermore, the cell viability reduced when MNPs were decorated with a SiO_2-coating layer, with a 56% reduction in the viability of cells exposed to a 4000 μg/mL suspension of Fe_3O_4@SiO_2 particles. The cell viability percentages at the determined concentrations for MIC (500 μg/mL) and MBC (1000 μg/mL) were estimated to be 81% and 76%, respectively. It was also found that the cell viability reduced up to 63%, following an exposure to Fe_3O_4@SiO_2 nanoparticles at concentrations about four- and twofold more remarkable than the MIC and MBC values, respectively. The cytotoxicity assay of free CS exhibited an exceptional biocompatibility even under exposure at the highest concentration (4000 μg/mL), with 80% of the cell viability and a superior biocompatibility behavior compared to other antimicrobial materials. The survey also demonstrated that modification of MNPs with chitosan could improve cytotoxicity compared to Fe_3O_4 and core/shell Fe_3O_4@SiO_2 particles. The lower toxicity of Fe_3O_4@SiO_2@CS nanocomposites may be due to the slower release of Fe^{+2} ions, which stimulates ROS-mediated cell death. The chitosan-modified Fe_3O_4@SiO_2 MNPs had a slightly toxic effect on cell viability even after exposure to extremely high concentrations as 71% cell viability was achieved at 4000 μg/mL, which was much higher than the concentrations required to induce bacteriostatic and bactericidal effects. The results obtained in this work revealed that free nisin had relatively nontoxic effects on the viability of mouse fibroblast cells. These findings also indicated that the nisin-functionalized nanocomposites could not suppress the growth of the fibroblast cells even after treatment to high nisin concentrations (12-768 μg/mL). These findings suggest a favorable biocompatibility of nisin and the modified nanostructures under *in vivo* conditions, with the viability values of 88% and 78% following exposure to a concentration of 768 μg/mL, respectively.

3.10. Animal Studies. Therapeutic efficacy of the Fe_3O_4@SiO_2@CS nanocomposites, nisin, and nisin-incorporated nanocomposites was assessed using male NMRI mice (6-8 weeks old) with VISA-infected wounds as models (Table 3). All formulations exhibited a considerable capacity in lowering the bacterial loads at excision sites, and in agreement with *in vitro* studies, nisin had the greatest efficiency, followed by nisin-modified nanostructures and then Fe_3O_4@SiO_2@CS. It was discovered that 9 days after the initial wound treatment, the nisin-treated groups had a bacterial burden of $7.8 \times 10^4 \pm 0.8 \times 10^4$ in the surgical incisions compared to those exposed to the nisin-loaded Fe_3O_4@SiO_2@CS and Fe_3O_4@SiO_2@CS nanocomposites, which contained the bacterial loads of about $2.2 \times 10^5 \pm 1.3 \times 10^5$ and $4.3 \times 10^5 \pm 1.2 \times 10^5$, respectively. According to Table 2, the bacterial load in the wound site was remarkably reduced after 14 days of exposure to all formulations, in comparison with the initial days of treatment as follows: 266 ± 18 CFU/mL was the VISA population of the groups treated with free nisin, the bacterial load amounted to 305 ± 25 CFU/mL in the groups of mice that received Fe_3O_4@SiO_2@CS-NISIN nanocomposites, and around 360 ± 14 CFU/mL in the groups treated with the Fe_3O_4@SiO_2@CS nanomaterials alone was observed. The superior performance of free nisin in suppressing the bacterial growth and wound healing process over other materials was also evident from the wound photographs (Figure 9), followed by nanocomposites containing nisin and Fe_3O_4@

Table 3: Bacterial counts (CFU/g) of a mouse skin abrasion lesion on the 4th, 9th, and 14th days after treatment.

Day	VISA	Free nisin	Fe_3O_4@SiO_2@CS	Fe_3O_4@SiO_2-CS-NISIN
0	3×10^7	5.5×10^7	5.6×10^7	5.5×10^7
4	Fatal	$5.7 \times 10^6 \pm 1.5 \times 10^6$	$5.8 \times 10^7 \pm 2.4 \times 10^7$	$4.8 \times 10^7 \pm 1.6 \times 10^7$
9	Fatal	$7.8 \times 10^4 \pm 0.8 \times 10^4$	$4.3 \times 10^5 \pm 1.2 \times 10^5$	$2.2 \times 10^5 \pm 1.3 \times 10^5$
14	Fatal	266 ± 18	360 ± 14	305 ± 25

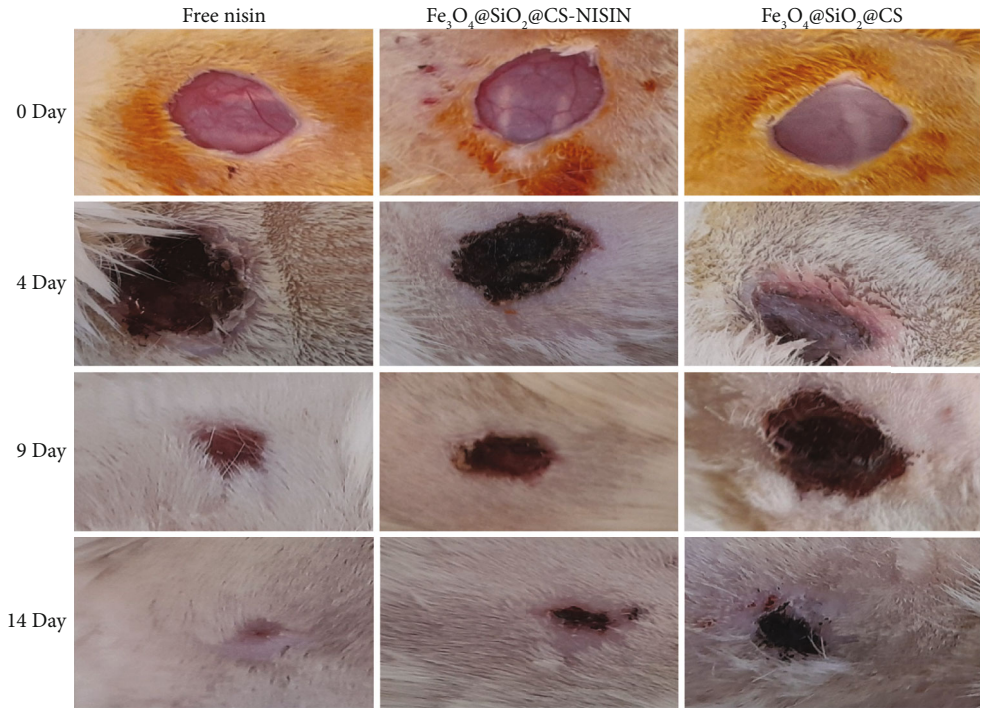

Figure 9: Photographs of wound healing process in the groups treated with free nisin, Fe_3O_4@SiO_2@CS-NISIN, and Fe_3O_4@SiO_2@CS groups on days 0, 4, 9, and 14 after skin injury.

SiO_2@CS. In this regard, the lower efficiency of nisin-decorated Fe_3O_4@SiO_2@CS composites than free nisin ($p < 0.05$) can be explained by the fact that some nisin molecules lose their function during the conjugation process. The results of the *in vivo* survey also revealed that the Fe_3O_4@-SiO_2@CS-NISIN nanocomposites and free nisin were more potent than the unmodified Fe_3O_4@SiO_2@CS composites in reducing the number of colonies during different time points ($p < 0.05$). The *in vivo* and *in vitro* antimicrobial efficiency of polycationic chitosan encapsulated with Fe_3O_4@SiO_2 can be attributed to the improvement of the mechanical strength and enhanced antibacterial properties and biocompatibility of the nanocomposites. Some researchers showed that a combination of the polymeric nanofibers with MNPs could enhance complementary mechanical and antibacterial properties to accelerate the wound healing process. In this regard, Cai et al. demonstrated that the introduction of Fe_3O_4 NPs into chitosan-gelatin (CS-GE) nanofiber matrix yielded a significant enhancement in the mechanical and antibacterial characteristics. It showed that an improvement in the loading content of Fe_3O_4 NPs from 1 to 4 w % led to an enhancement of Young's modulus and tensile strength values by 37% and 22%, respectively. It has been extensively reported that Young's modulus of materials can profoundly promote cell proliferation and differentiation, which are strongly correlated with the improved wound healing [47]. Wei et al. indicated that the efficient loading of rigid magnetic NPs (5%) into the composite polyvinyl alcohol-chitosan nanofibers (Fe_3O_4-PVA-CS) could contribute to the enhancement of Young's modulus from 48% to 57.4% and also the improvement in dynamics of cell attachment and growth due to the effective incorporation of Fe_3O_4 MNPs [48]. Some scientists reported that the TiO_2 NPs embedded into composite chitosan-pectin nanofibers and PVP- (poly (N-vinylpyrrolidone)-) chitosan nanofibers resulted in better antimicrobial efficiency and mechanical strength. It also observed a higher wound healing rate in comparison with chitosan-treated groups [49].

4. Discussion

The antibacterial property of Fe-O-based NPs is of special interest since the incidence and dissemination of strains

developing resistance to antibiotics are turning into a critical issue for public health threats throughout the world [50]. The potent inhibitory effect of Fe_3O_4 magnetic nanostructures has been confirmed on some Gram-positive and Gram-negative species, including *S. aureus*, *Xanthomonas*, *Escherichia coli*, and *Proteus vulgaris* [51–53]. Furthermore, Fe-O-based NPs are an economically beneficial biocide for various applications [54]. According to our findings, Fe_3O_4@SiO_2 MNPs exhibited good bacteriostatic and bactericidal effects at MIC and MBC values of 500 and 1000 μg/mL towards the VISA strain. The antibacterial effects of iron oxide NPs can stem from the release of Fe^{3+} ions, which are transported into the cell and interact with macromolecules such as proteins and DNA, impairing enzymatic activity, altering protein structures, and interrupting DNA strands. The Fe^{3+} ions also can effectively eliminate different bacterial species by the destruction of both cell walls and membranes due to their potent reducing effects [55]. The attachment of metal NPs to the bacterial cell surface triggers the generation of ROS such as superoxide (O^-_2) or hydroxyl radical (-OH), hydrogen peroxide (H_2O_2), and 1[O_2], which can ultimately lead to polysaccharide depolymerization, DNA strand breaks, lipid peroxidation, and enzyme inactivation [56, 57]. Nonoxidative mechanisms involve direct interaction and alteration of the integrity of the bacterial cell wall, allowing foreign molecules to penetrate and then covalently bind to proteins and cellular constituents, disrupting the normal function of the bacterial cell [58, 59]. The hydrodynamic diameters of the prepared nanostructures in this work were determined to be in the size ranges from 51 to 155 nm, with an obvious difference between DLS and SEM methods. We got smaller MNP sizes using SEM than those calculated by DLS. The MNPs with high volumes or surface areas allow delivery of a sufficient amount of drug molecules while preventing the recognition and immediate removal by RES systems. The nanostructures smaller than 5 nm may be fast eliminated from the bloodstream through renal filtration or liver excretion, whereas nanoparticles with sizes greater than 200 nm in diameter are efficiently cleared by the spleen or RES [60, 61]. Therefore, nanocarriers with diameters ranging from 20 to 200 nm can remain in the bloodstream for longer times because they can evade detection by the body's scavenger system [62]. A long-term systematic circulation period predicts a higher distribution of nanoparticles in the vicinity of target organs and accumulation to greater concentration [63]. The dependence of the antibacterial property of IONPs on the synthesis procedure was confirmed in several studies. We constructed Fe_3O_4 MNPs with a size of 20 nm in SEM using PEG-400 as an antibacterial agent, $FeCl_3$, and $FeCl_2$, when modified with a SiO_2 layer resulted in an effective inhibitory effect against VISA at MIC and MBC concentrations corresponding to 500 and 1000 μg/mL, respectively. In this regard, Fe_3O_4 MNPs prepared with the novel surfactant TWEEN80 and urea fuel with a size of about 35 nm displayed excellent inhibitory effects against both Gram-positive and Gram-negative bacterial strains [64]. In another work, the incorporation of *Malva sylvestris* in the synthesis of Fe_3O_4 NPs greatly improved the bacteriostatic and bactericidal effects against *S. aureus*, *Corynebacterium* sp., *Pseudomonas aeruginosa*, and *Klebsiella pneumonia* as compared to unmodified Fe_3O_4 MNPs [65]. Saqib et al. demonstrated the bactericidal performance of IONPs (25-40 nm) in the presence of predefined concentrations (50 and 100 μg/mL) against *S. aureus* and Gram-negative bacteria *Shigella dysenteriae* and *E. coli* with an inhibition zone of about 13 mm [66]. Al-Shabib et al. demonstrated that synthesized IONPs using PEG, $FeCl_3$, and $Fe_2(SO_4)_3$ oversize ranging of 6 to 9 nm had a high significant antibacterial property against a diverse array of Gram-negative and Gram-positive bacteria at different concentrations of MICs between 32 and 128 μg/mL, with a capacity to degrade the formation of biofilms and to destroy preformed biofilm structures [67]. The difference in antibacterial properties of IONPs can be attributed to the type of susceptible microorganisms, morphology and physicochemical characteristics of the nanocrystals, and the mechanism of antimicrobials action. Surface functionalization can also be an effective procedure for the improvement of the antibacterial capacity of Fe-O NPs. In this work, chitosan-coated MNPs had more pronounced antibacterial effects compared to Fe_3O_4@SiO_2, suggesting that the presence of chitosan on the surface of MNPs can improve the antibacterial properties of as-prepared MNPs. Incompatible with our findings, Arakha et al. showed that chitosan-coated IONPs could lead to the enhanced bactericidal activity of IONPs against *Bacillus subtilis* and *E. coli*, which correlated with the generation of ROS [68]. In another work, coating with chitosan significantly affected the antimicrobial propensity of Fe_3O_4 NPs against *Candida albicans*, *Aspergillus niger*, and *Fusarium solani* [69]. The most predominant proposed antibacterial effect of chitosan is based on its potential to attach with the negatively charged constituents of the bacterial cell wall and induce cell disruption, resulting in a change in membrane permeability [70], after which it attaches to DNA, leading to inhibition of DNA replication and protein synthesis and subsequent cell death [71]. Another possible mechanism is that chitosan molecules are capable of binding trace elements due to their chelating properties, thereby inhibiting the production of toxins and microbial growth [70]. In the present investigation, nisin exhibited a significantly high antibacterial efficacy when used at a concentration > 24 μg/mL. However, after exposure to nisin-modified Fe_3O_4@SiO_2@CS nanocomposites, the MIC and MBC values were approximately 5-fold lower than those of nisin alone (125 μg/mL), suggesting that several nisin molecules fail to exhibit antibacterial effects because of impaired functional activity during the conjugation process. Numerous investigations have indicated the prospects of antimicrobial peptides (AMPs) such as nisin in the treatment of bacterial infectious diseases [72–74]. The targeting mechanism of nisin involves a tight interaction with the negatively charged components in the bacterial surface structures and the formation of pores on cell membranes, which causes a change in cell membrane permeability and the efflux of small metabolites such as amino acids, nucleotides, ions, and other cytoplasm-solubilized substances [75] and also leads to the inhibition of peptidoglycan (PG) biosynthesis through the interaction with lipid II specific, resulting in cell death [76]. Jensen et al.

demonstrated the antimicrobial effects of nisin in the MIC range 6.4-12.8 μg/mL by damaging the cell membrane and disrupting chromosome replication or segregation in *S. aureus* [77]. Severina et al. found that nisin had a notable efficacy in the killing of a wide array of Gram-positive species, including MRSA, VRE, and *Streptococcus pneumonia* [78]. Additionally, a strain of *L. lactis* capable of nisin production was characterized as leading to reduced intestinal localization by VRE in a mouse infection model [79]. According to *in vivo* findings, the bacterial burden of wounds treated with nisin-coated Fe_3O_4@SiO_2@CS nanocomposites was $10^7(4.8 \pm 1.6)$, $10^5(2.2 \pm 1.3)$, and 305 ± 25 CFU/mL, whereas wounds exposed to free nisin had the bacterial loads of $10^6(5.7 \pm 1.5)$, $10^4(7.8 \pm 0.8)$, and 266 ± 18 CFU/mL, on the 4^{th}, 9^{th}, and 14^{th} days of the trial, respectively, which reduced inhibitory effects of nisin-modified nanocomposites relative to free nisin, indicating that the antibacterial effects of some nisin molecules were inhibited during the conjugation process ($p < 0.05$). The presence of glutaraldehyde molecules on the surface of the nanocomposites may have interfered with the binding of some nisin molecules to the VISA cell wall, or they may have blocked the nisin active sites. In line with our study, some researchers have also documented the *in vivo* antimicrobial and wound healing efficacy of nisin. Heunis et al. demonstrated the wound healing properties of nisin in a mouse model, where a nisin-containing nanofiber dressing remarkably affected wound closure and reduced the bacterial burden in the wound site, such that the number of surviving *S. aureus* cells was declined to 4.3×10^2 CFU/wound on day 7 following the exposure of nisin incorporated into nanofiber dressings, compared to 2.2×10^7 in wounds treated with control nanofiber wound dressings [80]. Following previous studies, Mouritzen et al. proposed nisin as a potential therapeutic tool to promote wound healing at a concentration of 25 μg/mL because of its immunomodulatory effect, robust functional efficiency against a variety of Gram-positive bacteria, and low cytotoxicity [81]. To determine the effect of compounds on cell viability, the *in vitro* cytotoxicity of nisin and nanocomposites on L-929 fibroblast cells was evaluated using a traditional MTT assay. The results showed extremely high cell viability (more than 85% even at a high concentration of 1 mg/mL) of L-929 cells treated with Fe_3O_4@SiO_2@CS nanocomposites, indicating remarkable cellular compatibility. Our findings reveal that the chitosan oligosaccharide coating onto Fe_3O_4 nanoparticles improves the viability of cells exposed to Fe_3O_4@SiO_2@CS magnetic nanocomposites compared to naked MNP treatment due to moderate ROS production. The lower cytotoxicity of Fe_3O_4@SiO_2@CS may correlate with the sustained release of Fe^{2+} ions, which trigger ROS-mediated cell death [82]. Similar results were also reported by Guo et al. who showed that Fe_3O_4@SiO_2 particles modified with DMSA can improve the cytotoxicity compared to Fe_3O_4 and Fe_3O_4@-SiO_2 magnetic particles. Furthermore, in line with this study, they found that cell cytotoxicity was enhanced when Fe_3O_4 MNPs were modified with a SiO_2 coating layer [83]. We displayed that free nisin and nisin-modified-Fe_3O_4@SiO_2@CS nanocomposites tested at concentrations ranging from 12 to 768 μg/mL had significantly favorable biocompatibility and can be safely used as the wound dressing.

5. Conclusions

Fe_3O_4@SiO_2 MNPs have been successfully embedded in a chitosan matrix to obtain Fe_3O_4@SiO_2@CS nanocomposites and then functionalized with nisin as an antimicrobial peptide (AMP), using a relatively efficient covalent linkage. All materials with particle sizes small sufficient and spherical shapes retained the magnetization properties. When chitosan-coated MNPs were applied, the antibacterial efficacy of the prepared nanocomposites exhibited a greater improvement than that of Fe_3O_4@SiO_2 alone, due to the high density of polycationic NH^+_3 groups in the chitosan structure and the strengthened interaction between the negatively charged components of the bacterial cells and the nanoparticles. Under both *in vivo* and *in vitro* settings, it was found that free nisin exerted a significantly higher inhibitory potency compared to Fe_3O_4@SiO_2@CS nanocomposites decorated with nisin against the VISA strain. This could be attributed to the inactivation of some nisin molecules during the conjugation process. The cytotoxicity results indicated that all the formulations had slightly significant effects on cell viability even at high concentrations, which may be greatly favorable for applying these magnetic nanocomposite materials in various biomedical fields.

Abbreviations

MNPs:	Magnetic nanoparticles
Fe_3O_4@SiO_2:	Silica-coated Fe_3O_4 magnetic nanoparticles
Fe_3O_4@SiO_2@CS:	Chitosan-coated Fe_3O_4@SiO_2 magnetic nanoparticles
Fe_3O_4@SiO_2@CS-NISIN:	Nisin-loaded Fe_3O_4@SiO_2@CS nanocomposites
XRD:	X-ray diffraction
FE-SEM:	Field emission scanning electron microscope
FTIR:	Fourier-transform infrared spectroscopy
DLS:	Dynamic light scattering
VSM:	Vibrating sample magnetometer
D_h:	Hydrodynamic diameter
DMEM:	Dulbecco's modified Eagle's media
FBS:	Fetal bovine serum
DMSO:	Dimethyl sulfoxide
MIC:	Minimum inhibitory concentration
MTT:	3-(4,5-Dimethylthiazol-2-yl)-2,5-diphenyltetrazolium bromide
MHB:	Mueller-Hinton broth
FDA:	Food and Drug Administration.

Data Availability

The datasets used and/or analyzed during the current study are available from the corresponding author on reasonable request.

Ethical Approval

This study was approved by the Ethics Committee of Hamadan University of Medical Sciences (Code No: IR.UMSHA.REC.1398.574).

Consent

Consent is not applicable.

Conflicts of Interest

The authors declare that they have no competing interests.

Acknowledgments

The authors are grateful to Hamadan University of Medical Sciences for their financial support in conducting the research (Grant/Award Number: 9808216062).

References

[1] D. Cameron, Y.-H. Lin, S. Trouillet-Assant et al., "Vancomycin-intermediate _Staphylococcus aureus_ isolates are attenuated for virulence when compared with susceptible progenitors," *Clinical Microbiology and Infection.*, vol. 23, no. 10, pp. 767–773, 2017.

[2] X. Zhu, C. Liu, S. Gao, Y. Lu, Z. Chen, and Z. Sun, "Vancomycin intermediate-resistant Staphylococcus aureus (VISA) isolated from a patient who never received vancomycin treatment," *International Journal of Infectious Diseases.*, vol. 33, pp. 185–190, 2015.

[3] Q. Hu, H. Peng, and X. Rao, "Molecular events for promotion of vancomycin resistance in vancomycin intermediate Staphylococcus aureus," *Frontiers in microbiology.*, vol. 7, p. 1601, 2016.

[4] P. G. Charles, P. B. Ward, P. D. Johnson, B. P. Howden, and M. L. Grayson, "Clinical features associated with bacteremia due to heterogeneous vancomycin-intermediate Staphylococcus aureus," *Clinical infectious diseases.*, vol. 38, no. 3, pp. 448–451, 2004.

[5] Y. Maor, M. Hagin, N. Belausov, N. Keller, D. Ben-David, and G. Rahav, "Clinical features of heteroresistant vancomycin-intermediate Staphylococcus aureus bacteremia versus those of methicillin-resistant S. aureus bacteremia," *The Journal of infectious diseases.*, vol. 199, no. 5, pp. 619–624, 2009.

[6] L.-C. Chen, W.-D. Chiang, W.-C. Chen et al., "Influence of alanine uptake on _Staphylococcus aureus_ surface charge and its susceptibility to two cationic antibacterial agents, nisin and low molecular weight chitosan," *Food chemistry.*, vol. 135, no. 4, pp. 2397–2403, 2012.

[7] J. Cai, J. Yang, C. Wang, Y. Hu, J. Lin, and L. Fan, "Structural characterization and antimicrobial activity of chitosan (CS-40)/nisin complexes," *Journal of Applied Polymer Science.*, vol. 116, no. 6, pp. NA–N7, 2010.

[8] S. M. Asaduzzaman and K. Sonomoto, "Lantibiotics: diverse activities and unique modes of action," *Journal of Bioscience and Bioengineering*, vol. 107, no. 5, pp. 475–487, 2009.

[9] A. J. van Heel, M. Montalban-Lopez, and O. P. Kuipers, "Evaluating the feasibility of lantibiotics as an alternative therapy against bacterial infections in humans," *Expert opinion on drug metabolism & toxicology.*, vol. 7, no. 6, pp. 675–680, 2011.

[10] P. D. Cotter, R. P. Ross, and C. Hill, "Bacteriocins – a viable alternative to antibiotics?," *Nature Reviews Microbiology.*, vol. 11, no. 2, pp. 95–105, 2013.

[11] J. M. Shin, I. Ateia, J. R. Paulus et al., "Antimicrobial nisin acts against saliva derived multi-species biofilms without cytotoxicity to human oral cells," *Frontiers in microbiology.*, vol. 6, p. 617, 2015.

[12] I. Hamed, F. Özogul, and J. M. Regenstein, "Industrial applications of crustacean by-products (chitin, chitosan, and chitooligosaccharides): a review," *Trends in food science & technology.*, vol. 48, pp. 40–50, 2016.

[13] S. F. Bruno, F. J. A. A. Ekorong, S. S. Karkal, M. Cathrine, and T. G. Kudre, "Green and innovative techniques for recovery of valuable compounds from seafood by-products and discards: a review," *Trends in Food Science & Technology.*, vol. 85, pp. 10–22, 2019.

[14] P. Watts, A. Smith, and M. Hinchcliffe, *ChiSys® as a chitosan-based delivery platform for nasal vaccination*, Mucosal Delivery of Biopharmaceuticals: Springer, 2014.

[15] S. Bonengel and A. Bernkop-Schnürch, "Thiomers – from bench to market," *Journal of Controlled Release*, vol. 195, pp. 120–129, 2014.

[16] A. G. Inanli, E. T. A. Tümerkan, N. El Abed, J. M. Regenstein, and F. Özogul, "The impact of chitosan on seafood quality and human health: a review," *Trends in Food Science & Technology.*, vol. 97, pp. 404–416, 2020.

[17] C. Y. Haw, F. Mohamed, C. Chia et al., "Hydrothermal synthesis of magnetite nanoparticles as MRI contrast agents," *Ceramics International*, vol. 36, no. 4, pp. 1417–1422, 2010.

[18] T. Alka and S. Neeraj, "Efficiency of superparamagnetic nano iron oxide loaded poly (acrylamide-co-acrylic acid) hydrogel in uptaking Pb 2 ions from water," *Journal of Dispersion Science and Technology*, vol. 27, pp. 1437–1444, 2013.

[19] R. Langer, "New methods of drug delivery," *Science*, vol. 249, no. 4976, pp. 1527–1533, 1990.

[20] S. Gul, S. B. Khan, I. U. Rehman, M. A. Khan, and M. Khan, "A comprehensive review of magnetic nanomaterials modern day theranostics," *Frontiers in Materials*, vol. 6, 2019.

[21] X. Li, Y. Wang, L. Shi et al., "Magnetic targeting enhances the cutaneous wound healing effects of human mesenchymal stem cell-derived iron oxide exosomes," *Journal of Nanobiotechnology*, vol. 18, no. 1, pp. 1–14, 2020.

[22] R. Roto, Y. Yusran, and A. Kuncaka, "Magnetic adsorbent of Fe_3O_4@SiO_2 core-shell nanoparticles modified with thiol group for chloroauric ion adsorption," *Applied Surface Science.*, vol. 377, pp. 30–36, 2016.

[23] W. Wu, Q. He, and C. Jiang, "Magnetic iron oxide nanoparticles: synthesis and surface functionalization strategies," *Nanoscale research letters.*, vol. 3, no. 11, pp. 397–415, 2008.

[24] S. Zhang, Y. Zhang, J. Liu et al., "Thiol modified Fe_3O_4@SiO_2 as a robust, high effective, and recycling magnetic sorbent for mercury removal," *Chemical Engineering Journal.*, vol. 226, pp. 30–38, 2013.

[25] J. Emerit, C. Beaumont, and F. Trivin, "Iron metabolism, free radicals, and oxidative injury," *Biomedicine & pharmacotherapy.*, vol. 55, no. 6, pp. 333–339, 2001.

[26] E. J. Van Den Bos, A. Wagner, H. Mahrholdt et al., "Improved efficacy of stem cell labeling for magnetic resonance imaging studies by the use of cationic liposomes," *Cell transplantation*, vol. 12, no. 7, pp. 743–756, 2003.

[27] M. Hofmann-Amtenbrink, H. Hofmann, and X. Montet, "Superparamagnetic nanoparticles–a tool for early diagnostics," *Swiss medical weekly.*, vol. 140, 2010.

[28] Y. Li, J. Liu, Y. Zhong et al., "Biocompatibility of Fe_3O_4@ Au composite magnetic nanoparticles in vitro and in vivo," *International Journal of Nanomedicine*, vol. 6, p. 2805, 2011.

[29] C. Sun, K. Du, C. Fang et al., "PEG-mediated synthesis of highly dispersive multifunctional superparamagnetic nanoparticles: their physicochemical properties and function in vivo," *ACS Nano*, vol. 4, no. 4, pp. 2402–2410, 2010.

[30] M. Gao, W. Li, J. Dong, Z. Zhang, and B. Yang, "Synthesis and characterization of superparamagnetic Fe_3O_4@SiO_2 core-shell composite nanoparticles," *World Journal of Condensed Matter Physics.*, vol. 1, no. 2, pp. 49–54, 2011.

[31] Z. Lei, X. Pang, N. Li, L. Lin, and Y. Li, "A novel two-step modifying process for preparation of chitosan-coated Fe_3O_4/SiO_2 microspheres," *Journal of Materials Processing Technology.*, vol. 209, no. 7, pp. 3218–3225, 2009.

[32] A. Esmaeili and S. Ghobadianpour, "Vancomycin loaded superparamagnetic $MnFe_2O_4$ nanoparticles coated with PEGylated chitosan to enhance antibacterial activity," *International Journal of Pharmaceutics*, vol. 501, no. 1-2, pp. 326–330, 2016.

[33] H. Wang, Y. She, C. Chu et al., "Preparation, antimicrobial and release behaviors of nisin-poly (vinyl alcohol)/wheat gluten/ZrO_2 nanofibrous membranes," *Journal of Materials Science*, vol. 50, no. 14, pp. 5068–5078, 2015.

[34] F. Behzadi, S. Darouie, S. M. Alavi et al., "Stability and antimicrobial activity of nisin-loaded mesoporous silica nanoparticles: a game-changer in the war against maleficent microbes," *Journal of agricultural and food chemistry.*, vol. 66, no. 16, pp. 4233–4243, 2018.

[35] E. Davies, H. Bevis, and J. Delves-Broughton, "The use of the bacteriocin, nisin, as a preservative in ricotta-type cheeses to control the food-borne pathogen Listeria monocytogenes," *Letters in Applied Microbiology.*, vol. 24, no. 5, pp. 343–346, 1997.

[36] V. Oluić-Vuković, "Bradford's distribution: from the classical bibliometric "law" to the more general stochastic models," *Journal of the American Society for Information Science.*, vol. 48, no. 9, pp. 833–842, 1997.

[37] M. Zohri, M. S. Alavidjeh, I. Haririan et al., "A comparative study between the antibacterial effect of nisin and nisin-loaded chitosan/alginate nanoparticles on the growth of Staphylococcus aureus in raw and pasteurized milk samples," *Probiotics and Antimicrobial proteins.*, vol. 2, no. 4, pp. 258–266, 2010.

[38] P. Prombutara, Y. Kulwatthanasal, N. Supaka, I. Sramala, and S. Chareonpornwattana, "Production of nisin-loaded solid lipid nanoparticles for sustained antimicrobial activity," *Food Control*, vol. 24, no. 1-2, pp. 184–190, 2012.

[39] CLSI C, "Performance standards for antimicrobial susceptibility testing," *Clinical Lab Standards Institute.*, vol. 35, no. 3, pp. 16–38, 2016.

[40] V. Baumans and P. Van Loo, "How to improve housing conditions of laboratory animals: the possibilities of environmental refinement," *The veterinary journal.*, vol. 195, no. 1, pp. 24–32, 2013.

[41] T. Saranya, K. Parasuraman, M. Anbarasu, and K. Balamurugan, "XRD, FT-IR and SEM study of magnetite (Fe_3O_4) nanoparticles prepared by hydrothermal method," *Nano Vision.*, vol. 5, no. 4-6, pp. 149–154, 2015.

[42] S. Aliramaji, A. Zamanian, and Z. Sohrabijam, "Characterization and synthesis of magnetite nanoparticles by innovative sonochemical method," *Procedia Materials Science*, vol. 11, pp. 265–269, 2015.

[43] Y. Liang, J. Ouyang, H. Wang, W. Wang, P. Chui, and K. Sun, "Synthesis and characterization of core-shell structured SiO_2@YVO_4:Yb^{3+},Er^{3+} microspheres," *Applied surface science.*, vol. 258, no. 8, pp. 3689–3694, 2012.

[44] H. Liu, F.-C. Yang, Y.-J. Tsai, X. Wang, W. Li, and C.-L. Chang, "Effect of modulation structure on the microstructural and mechanical properties of TiAlSiN/CrN thin films prepared by high power impulse magnetron sputtering," *Surface and coatings technology.*, vol. 358, pp. 577–585, 2019.

[45] M. Kasaeian, E. Ghasemi, B. Ramezanzadeh, M. Mahdavian, and G. Bahlakeh, "A combined experimental and electronic-structure quantum mechanics approach for studying the kinetics and adsorption characteristics of zinc nitrate hexahydrate corrosion inhibitor on the graphene oxide nanosheets," *Applied Surface Science.*, vol. 462, pp. 963–979, 2018.

[46] D. Sun, S. Kang, C. Liu, Q. Lu, L. Cui, and B. Hu, "Effect of zeta potential and particle size on the stability of SiO_2 nanospheres as carrier for ultrasound imaging contrast agents," *International Journal of Electrochemical Science*, vol. 11, no. 10, pp. 8520–8529, 2016.

[47] N. Cai, C. Li, C. Han et al., "Tailoring mechanical and antibacterial properties of chitosan/gelatin nanofiber membranes with Fe_3O_4 nanoparticles for potential wound dressing application," *Applied Surface Science.*, vol. 369, pp. 492–500, 2016.

[48] Y. Wei, X. Zhang, Y. Song et al., "Corrigendum: Magnetic biodegradable Fe_3O_4/CS/PVA nanofibrous membranes for bone regeneration (2011 Biomed. Mater. 6 055008)," *Biomedical Materials*, vol. 16, no. 1, p. 019501, 2021.

[49] D. Archana, J. Dutta, and P. Dutta, "Evaluation of chitosan nano dressing for wound healing: characterization, in vitro and in vivo studies," *International journal of biological macromolecules.*, vol. 57, pp. 193–203, 2013.

[50] S. V. Gudkov, D. E. Burmistrov, D. A. Serov, M. B. Rebezov, A. A. Semenova, and A. B. Lisitsyn, "Do iron oxide nanoparticles have significant antibacterial properties?," *Antibiotics*, vol. 10, no. 7, p. 884, 2021.

[51] N. Tran, A. Mir, D. Mallik, A. Sinha, S. Nayar, and T. J. Webster, "Bactericidal effect of iron oxide nanoparticles on Staphylococcus aureus," *International Journal of Nanomedicine*, vol. 5, pp. 277–283, 2010.

[52] A. Ebrahiminezhad, M. Zare, S. Kiyanpour, A. Berenjian, S. V. Niknezhad, and Y. Ghasemi, "Biosynthesis of xanthangum-coated INPs by using Xanthomonas campestris," *IET Nanobiotechnology.*, vol. 12, no. 3, pp. 254–258, 2018.

[53] S. Arokiyaraj, M. Saravanan, N. U. Prakash, M. V. Arasu, B. Vijayakumar, and S. Vincent, "Enhanced antibacterial activity of iron oxide magnetic nanoparticles treated with _Argemone mexicana_ L. leaf extract: an in vitro study," *Materials Research Bulletin.*, vol. 48, no. 9, pp. 3323–3327, 2013.

[54] U. S. Ezealigo, B. N. Ezealigo, S. O. Aisida, and F. I. Ezema, "Iron oxide nanoparticles in biological systems: antibacterial and toxicology perspective," *JCIS Open.*, vol. 4, p. 100027, 2021.

[55] S. Stankic, S. Suman, F. Haque, and J. Vidic, "Pure and multi metal oxide nanoparticles: synthesis, antibacterial and cytotoxic properties," *Journal of Nanobiotechnology*, vol. 14, no. 1, pp. 1–20, 2016.

[56] L. Wang, C. Hu, and L. Shao, "The antimicrobial activity of nanoparticles: present situation and prospects for the future," *International Journal of Nanomedicine*, vol. Volume 12, pp. 1227–1249, 2017.

[57] E. D. Weinberg, "Iron loading and disease surveillance," *Emerging infectious diseases.*, vol. 5, no. 3, pp. 346–352, 1999.

[58] A. Sarwar, H. Katas, S. N. Samsudin, and N. M. Zin, "Regioselective sequential modification of chitosan via azide-alkyne click reaction: synthesis, characterization, and antimicrobial activity of chitosan derivatives and nanoparticles," *PLoS One*, vol. 10, no. 4, article e0123084, 2015.

[59] P. V. Baptista, M. P. McCusker, A. Carvalho et al., "Nano-strategies to fight multidrug resistant bacteria—"a battle of the titans"," *Frontiers in microbiology.*, vol. 9, p. 1441, 2018.

[60] S. Parveen, R. Misra, and S. K. Sahoo, "Nanoparticles: a boon to drug delivery, therapeutics, diagnostics and imaging," *Nanomedicine: Nanotechnology, Biology and Medicine.*, vol. 8, no. 2, pp. 147–166, 2012.

[61] N. Bertrand, J. Wu, X. Xu, N. Kamaly, and O. C. Farokhzad, "Cancer nanotechnology: the impact of passive and active targeting in the era of modern cancer biology," *Advanced drug delivery reviews.*, vol. 66, pp. 2–25, 2014.

[62] S. E. Gratton, P. A. Ropp, P. D. Pohlhaus et al., "The effect of particle design on cellular internalization pathways," *Proceedings of the National Academy of Sciences.*, vol. 105, no. 33, pp. 11613–11618, 2008.

[63] Y. Liu, M. Li, F. Yang, and N. Gu, "Magnetic drug delivery systems," *Science China Materials*, vol. 60, no. 6, pp. 471–486, 2017.

[64] Y. Prabhu, K. V. Rao, B. S. Kumari, V. S. S. Kumar, and T. Pavani, "Synthesis of Fe_3O_4 nanoparticles and its antibacterial application," *International Nano Letters.*, vol. 5, no. 2, pp. 85–92, 2015.

[65] S. M. Mousavi, S. A. Hashemi, M. Zarei et al., "Data on cytotoxic and antibacterial activity of synthesized Fe_3O_4 nanoparticles using _Malva sylvestris_," *Data in brief.*, vol. 28, article 104929, 2020.

[66] S. Saqib, M. F. H. Munis, W. Zaman et al., "Synthesis, characterization and use of iron oxide nano particles for antibacterial activity," *Microscopy research and technique.*, vol. 82, no. 4, pp. 415–420, 2019.

[67] N. A. Al-Shabib, F. M. Husain, F. Ahmed et al., "Low temperature synthesis of superparamagnetic iron oxide (Fe_3O_4) nanoparticles and their ROS mediated inhibition of biofilm formed by food-associated bacteria," *Frontiers in microbiology.*, vol. 9, p. 2567, 2018.

[68] M. Arakha, S. Pal, D. Samantarrai et al., "Antimicrobial activity of iron oxide nanoparticle upon modulation of nanoparticle-bacteria interface," *Scientific Reports*, vol. 5, no. 1, pp. 1–12, 2015.

[69] P. Nehra, R. Chauhan, N. Garg, and K. Verma, "Antibacterial and antifungal activity of chitosan coated iron oxide nanoparticles," *British journal of biomedical science.*, vol. 75, no. 1, pp. 13–18, 2018.

[70] R.-C. Chien, M.-T. Yen, and J.-L. Mau, "Antimicrobial and antitumor activities of chitosan from shiitake stipes, compared to commercial chitosan from crab shells," *Carbohydrate polymers.*, vol. 138, pp. 259–264, 2016.

[71] G. Yuan, H. Lv, W. Tang, X. Zhang, and H. Sun, "Effect of chitosan coating combined with pomegranate peel extract on the quality of Pacific white shrimp during iced storage," *Food Control*, vol. 59, pp. 818–823, 2016.

[72] J. J. Ahire and L. M. Dicks, "Nisin incorporated with 2, 3-dihydroxybenzoic acid in nanofibers inhibits biofilm formation by a methicillin-resistant strain of Staphylococcus aureus," *Probiotics and antimicrobial proteins.*, vol. 7, no. 1, pp. 52–59, 2015.

[73] S. Dosler and A. A. Gerceker, "In vitro activities of nisin alone or in combination with vancomycin and ciprofloxacin against methicillin-resistant and methicillin-susceptible Staphylococcus aureus strains," *Chemotherapy*, vol. 57, no. 6, pp. 511–516, 2012.

[74] K.-i. Okuda, T. Zendo, S. Sugimoto et al., "Effects of bacteriocins on methicillin-resistant Staphylococcus aureus biofilm," *Antimicrobial agents and chemotherapy.*, vol. 57, no. 11, pp. 5572–5579, 2013.

[75] P. Zimet, Á. W. Mombrú, R. Faccio et al., "Optimization and characterization of nisin-loaded alginate-chitosan nanoparticles with antimicrobial activity in lean beef," *LWT.*, vol. 91, pp. 107–116, 2018.

[76] E. Breukink and B. de Kruijff, "Lipid II as a target for antibiotics," *Nature reviews Drug discovery.*, vol. 5, no. 4, pp. 321–323, 2006.

[77] C. Jensen, H. Li, M. Vestergaard, A. Dalsgaard, D. Frees, and J. J. Leisner, "Nisin damages the septal membrane and triggers DNA condensation in methicillin-resistant Staphylococcus aureus," *Frontiers in Microbiology.*, vol. 11, p. 1007, 2020.

[78] E. Severina, A. Severin, and A. Tomasz, "Antibacterial efficacy of nisin against multidrug-resistant Gram-positive pathogens," *The Journal of antimicrobial chemotherapy.*, vol. 41, no. 3, pp. 341–347, 1998.

[79] M. Millette, G. Cornut, C. Dupont, F. Shareck, D. Archambault, and M. Lacroix, "Capacity of human nisin- and pediocin-producing lactic acid bacteria to reduce intestinal colonization by vancomycin-resistant enterococci," *Applied and Environmental Microbiology.*, vol. 74, no. 7, pp. 1997–2003, 2008.

[80] T. D. Heunis, C. Smith, and L. M. Dicks, "Evaluation of a nisin-eluting nanofiber scaffold to treat Staphylococcus aureus-induced skin infections in mice," *Antimicrobial agents and chemotherapy.*, vol. 57, no. 8, pp. 3928–3935, 2013.

[81] M. V. Mouritzen, A. Andrea, K. Qvist, S. S. Poulsen, and H. Jenssen, "Immunomodulatory potential of nisin A with application in wound healing," *Wound Repair and Regeneration.*, vol. 27, no. 6, pp. 650–660, 2019.

[82] S. Shukla, A. Jadaun, V. Arora, R. K. Sinha, N. Biyani, and V. Jain, "_In vitro_ toxicity assessment of chitosan oligosaccharide coated iron oxide nanoparticles," *Toxicology reports.*, vol. 2, pp. 27–39, 2015.

[83] X. Guo, F. Mao, W. Wang, Y. Yang, and Z. Bai, "Sulfhydryl-modified Fe_3O4@ SiO_2 core/shell nanocomposite: synthesis and toxicity assessment in vitro," *ACS applied materials & interfaces.*, vol. 7, no. 27, pp. 14983–14991, 2015.